QUANTITATIVE INFRARED THERMOGRAPHY AND CONVECTIVE HEAT TRANSFER MEASUREMENTS

Giovanni Maria Carlomagno

Università degli Studi di Napoli "Federico II", Dipartimento di Energetica, Termofluidodinamica Applicata e Condizionamenti Ambientali (D.E.T.E.C.)
P.le Tecchio 80, 80125 Napoli, ITALY

Infrared (IR) thermography is a two-dimensional, non-contact technique of temperature measurement which can be usefully exploited in a vast variety of industrial applications as well as research fields [1-9]. The infrared scanning radiometer (IRSR) basically includes a camera which detects the electromagnetic energy radiated in the infrared spectral band by an object (whose surface temperature is to be measured) and converts it into an electronic video signal. This signal corresponds to the object temperature map.

In the present work, attention is focused on the capability of IRSR to measure heat transfer coefficients in three different fluid flow configurations; in particular, the heat transfer to a jet centrally impinging on a rotating disk; the complex heat transfer pattern associated with a jet in cross-flow; the heat transfer distribution along a 180deg turn channel.

For all the aforementioned applications, the convective heat transfer coefficient from the model surface to the flowing stream is measured by making use of the so-called *heated-thin-foil* technique. This technique consists of uniformly heating a thin metallic foil (or a printed circuit board) by Joule effect and measuring at steady state the convective heat transfer coefficient h by means of the relationship:

$$h = \frac{\dot{q} - \dot{q}_l}{T_w - T_{aw}} \tag{1}$$

where: $\dot{q}$ is the known Joule heating flux, $\dot{q}_l$ represents thermal losses which are mainly due to tangential conduction along the foil $\dot{q}_c$ and radiation $\dot{q}_r$, T_w is the wall temperature which is measured when heating the foil (hot image) and T_{aw} is the adiabatic wall temperature (without heating, cold image). The tangential conduction $\dot{q}_c$, which modulates the thermal signal, may be evaluated by means of the second derivative of the wall temperature T_w while the thermal losses $\dot{q}_r$ may be evaluated according to the Stefan-Boltzmann law. The former may be relatively important even though is generally neglected because of the lack of a detailed temperature map which is instead accomplished with infrared thermography.

Data is reduced in non-dimensional form in terms of the Nusselt number Nu and presented as maps of Nu, or Nu normalized with a reference Nusselt number value which will later be specified.

Jet impinging on a rotating disk

Many works [10-15] deal with the heat exchanged by a disk rotating in still air, otherwise the interaction of an air jet with the flow generated by the disk has received only little attention [16-18].

The physical phenomenon is characterized by Reynolds and Nusselt numbers based on both the disk conditions Nu_r and Re_r and the jet conditions Re_j , Nu_j:

$$Re_r = \frac{\omega r^2}{\nu} \tag{2}$$

$$Re_j = \frac{U_j D}{\nu} \tag{3}$$

$$Nu_j = \frac{hD}{k} \tag{4}$$

$$Nu_r = \frac{hr}{k} \tag{5}$$

where ω is the rotating speed of the disk, r is the local disk radius, U_j is the jet velocity, D is the nozzle exit diameter, ν and k are respectively the kinematic viscosity and the thermal conductivity of air, h is defined by eq.(1).

In order to evaluate the relative importance of the jet effect with respect to the disk rotation and on the assumption that the heat transfer coefficient is proportional to the momentum flux, a possible similitude parameter which may represent the ratio between the two momentum fluxes, one due to the jet and the other one to the disk rotation, can be searched for.

The momentum rate of the jet, is obviously proportional to:

$$\rho V D^2 V \tag{6}$$

while the rate of momentum induced by the rotating disk may be assumed proportional to:

$$\rho \omega r \; r\delta \; \omega r \tag{7}$$

where δ is the local boundary layer thickness. Of course, an appropriate local radius r has to be chosen.

The present testing conditions include relatively high values of impingement distance z and as it is well known, under these circumstances, the width of the jet is proportional to the distance from the nozzle.

By taking into account that, for laminar flow on a rotating disk, the boundary layer thickness is constant and proportional to the square root of the ratio between the kinematic viscosity coefficient and the angular speed of the disk and by substituting in (7) the local radius with the semi-width of the jet (which in turn is proportional to z) the searched similitude parameter, proportional to the momentum rates ratio, may be put in the form:

$$\xi^2 = Re_j^2 \left(\frac{\nu}{\omega z^2} \right)^{3/2} = \frac{Re_j^2}{Re_r^{3/2} \left(\frac{z}{r} \right)^3} \tag{8}$$

In the present experiment, the disk section consists of a 450*mm* OD steel cup filled with a 20*mm* polyurethane foam on which a thin heating printed circuit board is glued; a small centred jet impinges on it [19].

The disk speed is varied in the laminar range (Re_r <250 000), the parameter ξ ranges from 0.1 to 100; three nozzles of exit diameter 4, 6 and 8*mm* are employed and their distance from the disk is varied between 15 and 75 nozzle diameters. The bulk temperature of the jet is kept practically equal to the temperature of the ambient air it mixes with and, because of the relatively low Mach number, the adiabatic wall temperature is considered to coincide with the ambient temperature and consequently with the jet bulk one.

For $0.1 \leq \xi \leq 1$, present data leads to a correlation between the Nusselt number and the Reynolds number at the disk centre (stagnation point) that can be written as:

$$\left(\frac{Nu_r}{\sqrt{Re_r}}\right)_{r=0} - 0.33 = 1.58\xi \tag{9}$$

which has a good correlation coefficient (R^2 = 0.988) and, for $\xi \to 0$, reduces to the classical relationship between the local Nusselt and Reynolds numbers for a laminar boundary layer over a rotating disk [15]. Instead for $1 \leq \xi \leq 100$ data is well correlated by equation:

$$\left(\frac{Nu_r}{\sqrt{Re_r}}\right)_{r=0} - 0.33 = 0.28 + 1.59\xi^{0.62} \tag{10}$$

The two above correlations are shown in Fig.1 together with the experimental measurements.

For ξ >2, all the experimental profiles of the heat transfer coefficient along the disk radius, reported in terms of the dimensionless parameter $\left(\frac{Nu_r}{\sqrt{Re_r}}\right)$ normalised with respect to $\left(\frac{Nu_r}{\sqrt{Re_r}}\right)_{r=0}$ against *r/z*, tend to overlap for *r/z* < 0.8. However, for increasing *r/z* and according to the tested conditions, most of the curves show an increasing convective heat transfer coefficient; this effect may be ascribed to the interaction of the turbulent jet with the laminar boundary layer generated by the rotating disk that, inducing an earlier transition, enhances the heat exchange at high *r/z*.

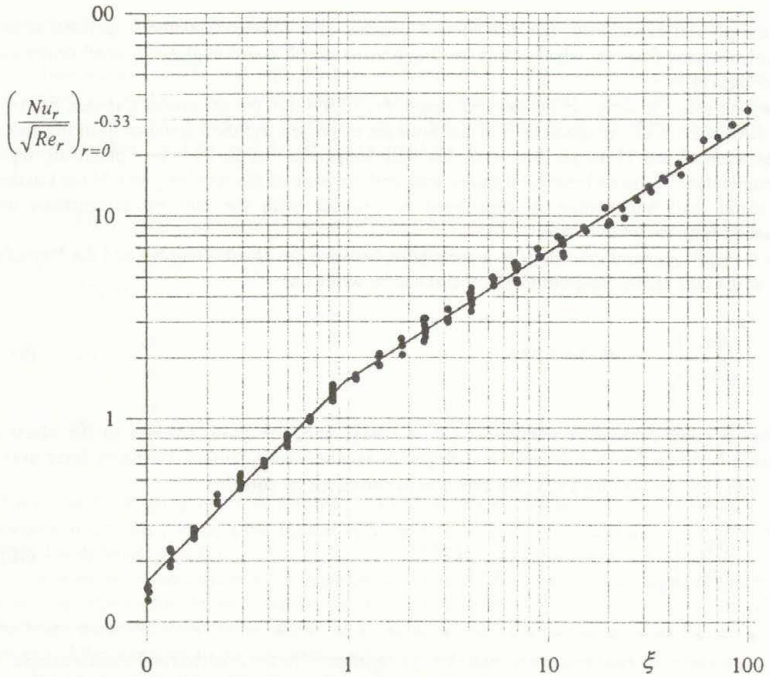

Fig.1 – Experimental data correlation

Jet in cross-flow

The study of a jet in cross-flow is attractive because of the vast engineering applications which include, among others, lifting jets for V/STOL aircraft during transition flight, turbine blade cooling, chimney plumes for the dispersion of pollutants into atmosphere. However, the main efforts of previous works [20-24] have been mainly focused on the comprehension of flow field dynamics, with little attention to heat transfer mechanisms [25], while a jet in cross-flow is a fundamental aspect of cooling problems.

In this work, measurements of the convective heat transfer coefficients over a flat plate due to the combined effects of the free stream and the jet perpendicularly injected into the cross stream are performed for varying the stream velocity, U_∞ between 5 and 10 *m/s* and the injection ratio, $R = U_j / U_\infty$, where U_j is the jet mean velocity at nozzle exit, between 1 and 5.

Tests are carried out in an open circuit wind tunnel characterized by a test section $300 \times 400 mm^2$ and a very low turbulence level (≅0.1%). One side wall of the tunnel is made of a thin printed circuit board (600*mm* long) insulated at its back and with a centred hole, drilled at 200*mm* from the plate edge (i.e. the tunnel throat), for the jet injection; the electrical continuity for the Joule heating is

assured by welding points over the copper tracks (4.5*mm* wide) near the hole edge. The access window to the test section for the infrared camera is simply made of bioriented polyethylene; calibration of the radiometer takes into account its presence. The air jet issues from a circular nozzle of exit diameter D =13.7*mm*; air, supplied by a compressor, goes through a pressure-regulating valve, a heat exchanger, a flow-meter, then to a plenum chamber (where its temperature is metered) and so through the nozzle into the wind tunnel section. Particular care is taken to maintain, during tests, the plenum jet temperature equal to the ambient one, which coincides with the stream temperature.

A typical result is presented in Fig.2 as a map of Nu/Nu_o, where Nu_o is the measured Nusselt number relative to the undisturbed plate without jet injection and with the hole closed to simulate the case of a flat plate; a circle denotes the position of the jet exit. In general, Nu/Nu_o takes values equal to unity outside the jet wake where heat transfer is influenced only by the stream. Immediately downstream of the injection hole a low heat transfer zone is present and further downstream the Nusselt number increases attaining its maximum value at about X/D =1.75 starting from the nozzle centre. A secondary peak, less pronounced than the first one is located at about 3.25 diameters downstream.

According to literature, the minimum heat transfer value at about 1D may be ascribed to the stagnation region created by the injection. The maximum instead may be associated with the formation of eddies in the wake region; in fact for increasing R, as the jet separates from the wall, the mainstream flow penetrates beneath the jet giving rise to the formation of the wake vortices which entail high local heat transfer. The two lateral Nu/Nu_o minima at about 1D should correspond to the position of the two trailing vortices which accompany the jet issuing from the nozzle.

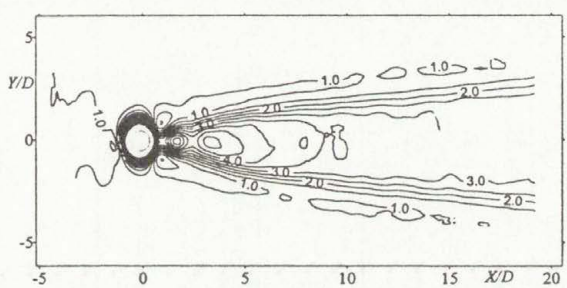

Fig.2 - Nu/Nu_o map for R=3

180deg turn channel

The thermal behaviour of a fluid into 180deg turn channels has been the subject matter of many experiments, as well numerical, studies [26-28] because of the relevant industrial application to turbine blade cooling.

A two-pass square channel of cross section 80x80mm^2 and 2000*mm* long before the turn is tested; these dimensions ensure a hydrodynamically fully developed flow ahead of the 180deg turn. The central partition wall between the two adjacent ducts is 16*mm* thick and ends with a square tip which is 80*mm* distant from the short side of the channel.

The channel walls are manufactured from wood apart from the two side walls, starting from the turn and for a length of about 1200*mm*, which are made each of them of printed circuit boards

joined together and connected in series. Two different kinds of circuit are considered. The first circuit is manufactured with copper tracks which are $17\mu m$ thick, $3mm$ wide, placed at $3.2mm$ pitch and also aligned with the axes of the ducts; each board is $400mm$ long. The second circuit instead is manufactured with copper tracks that are $5\mu m$ thick, $1.73mm$ wide, placed at $2mm$ pitch and aligned with the axes of the ducts; each board is $600mm$ long. The printed circuits are designed so as to achieve a constant heat flux over their surface (except beneath the partition wall) by Joule effect and, therefore, the thickness and width of their conducting tracks are manufactured with very close tolerances. A stabilised DC power source supplies the electric current to the circuit and the power input is monitored by precisely measuring voltage drop and current across the circuit.

The heat transfer coefficient is calculated by means of Eq.(1) where $T_{aw} = T_b$. In this case T_b is the stream bulk temperature which is evaluated by measuring the stagnation temperature at the channel entrance and by making a one-dimensional energy balance along the channel. Data is reduced in non-dimensional form in terms of the Nusselt number Nu. Both the Nusselt number and the Reynolds number are based on the channel hydraulic diameter.

The distribution of the local Nusselt number Nu in the vicinity of the turn, normalized by its fully developed counterpart Nu^* (Dittus-Boelter correlation) is reported in Fig.3 for $Re_d = 30\,000$. In more details, Fig.3a) refers to the first circuit type, while Fig.3b) and c) to the second circuit without (b) and with (c) correction for tangential conduction.

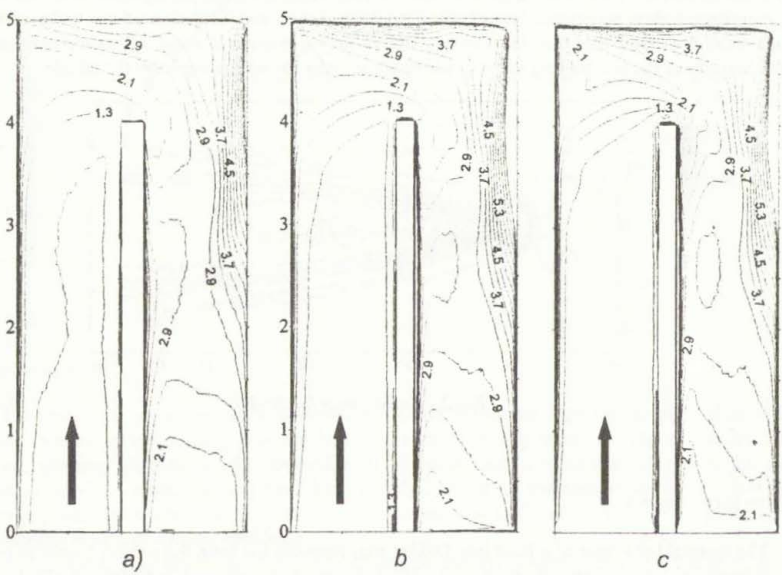

Fig.3 - Nu/Nu^* maps for Re_d =30 000

Generally, by moving streamwise along the heated zone of the channel Nu/Nu^* increases around the turn and downstream of it because of secondary flows. Three high heat transfer regions may be recognised: the first one is located by the end wall (in front of the partition wall towards the first outer corner) and is caused by the jet coming from the first duct which impinges on this wall; the second one is located downstream of the second corner of the outer wall and is due to the *jet*

effect of the flow through the bend; the third one is located at about the half part of the partition wall, downstream of the second inner corner, where the flow *rebounding* from the outer wall, impinges before exhaust. The second zone attains Nu/Nu^* values greater than the other two. Two relatively low heat transfer zones are also observed, one just before the first corner of the outer wall and the other one in the neighbourhood of the tip of the partition wall; these zones make evidence of the existence of recirculation bubbles. Another small zone, exhibiting a low heat transfer coefficient, is positioned nearby the end wall, practically across the exhaust duct axis.

The influence of the type of circuit lies essentially in the different tangential conduction value which is due to the different copper tracks thickness. By comparing maps (a) and (b) both without correction it is clearly evident as the zones of high and low heat transfer are more visible in the second case; these zones become further more visible when (c) the tangential conduction correction is made.

Results from the three fluid flow configurations demonstrate the capability of infrared thermography to deal with complex flow dynamics, the interaction between the jet and the boundary layer linked to the disk rotation, heat transfer developing in the wake of region of a jet in cross-flow, high heat transfer regions and recirculation bubbles in a 180deg turn channel.

References

1. G.M. Carlomagno and L. de Luca, Infrared Thermography in Heat Transfer in *Handbook of Flow Visualization*, (ed. W.J. Yang) chap. 32, pp. 531-553, Hemisphere, 1989.
2. G.M. Carlomagno, Heat transfer measurements by means of infrared thermography, in Measurement Techniques, von Karman Institute for Fluid Mechanics Lect. Series 1993-05, 1-114, Rhode-Saint-Genese, 1993.
3. G. Simeonides, P. Van Lierde, S. Van der Stichele, D. Capriotti and J.F. Wendt, Infrared Thermography in Blowdown and Intermittent Hypersonic Facilities, *AIAA Paper* 89-0042, 1989.
4. A. Henckels, F. Maurer, H. Olivier and H. Grönig, Fast Temperature Measurement by Infrared Line Scanning in a Hypersonic Shock Tunnel, *Experiments in Fluids*, vol. 9, pp. 298-300, 1990.
5. L. de Luca, G.M. Carlomagno and G. Buresti, Boundary Layer Diagnostics by Means of an Infrared Scanning Radiometer, *Experiments in Fluids,* vol. 9, pp.121-128, 1990.
6. D.L. Balageas, D.M. Boscher, A.A. Déom, J. Fournier and G. Gardette, Measurement of Convective Heat Transfer Coefficients in Wind Tunnels using Passive and Stimulated Infrared thermography, *Rech. Aerosp.*, 1991-4, pp.51-72, 1991.
7. G.M. Carlomagno, L. de Luca and T. Alziary de Roquefort, Mapping and Measurement of Aerodynamic Heating and Surface Flow Visualization by means of IR Thermography, in Multiphase Flow and Heat Transfer, (eds. X.J. Chen et al.), vol. 2, pp. 1316-1324, Hemisphere, 1991.
8. D.S. Bynum, F.K. Hube, C.M. Key and P.M. Diek, Measurement and Mapping of Aerodynamic Heating with an Infrared Camera, AEDC Rept. TR-76-54, pp.1-33, 1976.
9. G.M. Carlomagno, Thermofluid-Dynamics Applications of Quantitative Infrared Thermography, *Journal of Flow visualization and Image Processing*, vol. 4, pp. 261-280, 1997.
10. C. Wagner, Heat Transfer from a Rotating Disk to Ambient Air, *J. Applied Physics*, vol.19, pp.837-839, 1948.
11. K. Millsaps and K. Pohlhausen, Heat Transfer by Laminar Flow from a Rotating Plate, *J. Aeronautical Science*, vol.19, pp.120-126, 1952.

12. E.C. Cobb and O.A. Saunders, Heat Transfer from a Rotating Disk, *Proc. Royal Society,* vol. 236, pp. 343-351, 1956.
13. Cz.O. Popiel and L. Boguslawski, Local Heat Transfer Coefficients on the Rotating Disk in Still Air, *Int. J. Heat Mass Transfer*, vol.18, pp. 167-170, 1975.
14. A. Norhrop and J.M. Owen, Heat Transfer Measurements in Rotating-disk Systems, Part 1: The Free Disk, *Int. J. Heat and Fluid Flow*, vol.9, n°1, pp. 19-26, 1988.
15. G. Cardone, T. Astarita and G.M. Carlomagno, Heat Transfer Measurements on a Rotating Disk, *Int. J. Rotating Machinery*, Vol. 3, 1997.
16. S. Brodersen, D.E. Metzger and H.J.S. Fernando, Flows Generated by the Impingement of a Jet on a Rotating Surface, Part I-Basic Flow Patterns, *J. of Fluid Engineering*, Vol.118, 1996.
17. S. Brodersen, D.E. Metzger and H.J.S. Fernando, Flows Generated by the Impingement of a Jet on a Rotating Surface: Part II-Detailed Flow Structure and Analysis, *J. of Fluid Engineering*, Vol.118, 1996.
18. D.E. Metzger, W.J. Mathis and L.D. Grochowsky, Jet Cooling at the Rim of a Rotating Disk, *J. of Engineering for Power*, Vol.101, 1979.
19. T. Astarita, G. Cardone, and G.M. Carlomagno, Heat Transfer Measurements on a Rotating Disk with a Centred Impinging Jet, *Proc. Int. Symp. on Flow Visualization*, G.M. Carlomagno and I. Grant eds., paper n. 268, Sorrento, 1998.
20. J. Andreopoulos and W. Rodi, Experimental Investigation of Jets in a Crossflow, *J. Fluid Mech.* Vol. 138, pp. 93-127, 1984.
21. R.L. Sykes, W.S. Lewellen and S.F. Parker, On the Vorticity Dynamics of a Turbulent Jet in a Crossflow, *J. Fluid Mech.* Vol. 168, pp. 393-413, 1986.
22. S.L.V. Coelho, and J.C.R. Hunt, The Dynamics of the Near Field of Strong Jets in Crossflows, *J. Fluid Mech.* Vol. 200, pp. 95-120, 1989.
23. R.M. Kelso, T.T. Lim and A.E. Perry, An Experimental Study of Round Jets in Cross-flow, *J. Fluid Mech.* Vol. 306, pp. 111-144, 1996.
24. G.M. Carlomagno, A. Cenedese, and G. De Angelis, PTV Analysis of Jets in Cross-flow, *Proceedings of 9th Intern. Symp. on Applications of Laser Techniques to Fluid Mechanics,* vol.2, 38.3 1-38.3 7, Lisbon, 1998.
25. R.J. Goldstein, and J.R. Taylor, Mass Transfer in the Neghborhood of Jets Entering a Crossflow, *J. Heat Transfer* vol.104, pp. 715-721, 1982.
26. M.K. Chyu, Regional Heat Transfer in Two-Pass and Three-Pass Passages with 180-deg Sharp Turns, *ASME Journal of Heat Transfer,* vol.113, pp.63-70, 1991.
27. T. Arts, M. Lambert de Rouvroit, G. Rau and P. Acton, Aero-Thermal Investigation of the Flow Developing in a 180 Degree Turn Channel, *Proc. Int. Symp. on Heat Transfer in Turbomachinery,* Athens, 1992.
28. S.C. Lau, L.M. Russell, D.R. Thurman and S.A. Hippensteele, Visualization of Local Heat Transfer in Serpentine Channels with Liquid Crystals, *Proc. V Int. Symp. on Transport Phenomena and Dynamics of Rotating Machinery,* vol. A, pp. 411-423, Kaanapaly, Hawaii, 1994.

IMAGE PROCESSING PROBLEMS IN FLUID MECHANICS

Ian Grant,
Fluid Loading and Instrumentation Centre,
Heriot Watt University, Edinburgh EH14 4AS, Scotland, UK

SUMMARY

Image processing in fluid mechanics, often in conjunction with quantitative flow visualisation, is now an important tool used in experimental studies. The development of inexpensive, powerful image capture and processing hardware is being complemented by imaginative software development, both utilising ideas developed from optical image processing and evolving new concepts based on advances in computation and electronic publication. The present paper reviews these developments with emphasis on computation and electronic presentation.

INTRODUCTION

Image processing is now primarily understood as digital in nature. In fact, electronic digital pictures first became of interest when newspaper images were exchanged between London and New York by submarine cable in the 1920's. The mid 1960's saw the application of digital image processing when third-generation digital computers began to offer the speed and storage capabilities necessary for practical implementation of image processing algorithms [1]. The use of analogue, and in particular optical, image processing methods (using both coherent and incoherent sources) has a long history of diligent ingenuity. The diffraction pattern as a Fourier transform of the aperture producing the diffraction and spatial filtering using the pattern and an inverse optical transform is just one important example. The use of optical processing concurrently with digital processing was in evidence in early PIV studies in order to compensate for limited digital computational speed.

The development of inexpensive and effective (computer) electronic peripheral hardware dedicated to image capture and processing in the last ten years had taken the subject of flow visualisation and digital image processing from being the province of the largest best-funded laboratories and made it available to most experimentalists.

Parallel developments have taken place in electronic publishing leading to near universal access to the World Wide Web (WWW) and the opportunity to use the Web as a means of publication without necessarily undergoing peer review. Nevertheless, since fluid mechanics concerns the visual observation of dynamic processes, the possibility, in electronic media, to use digital video and synthetic moving images offers the opportunity to convey immediate impressions both of the science, and the excitement of the subject.

The use of WWW search engines using keywords such as 'flow visualization' or Boolean searches such as 'image processing' AND 'flow' will produce many hundreds of 'hits' if the main search engines / data bases are used (see example list at end of paper). Alternative means of electronic publication, also benefiting from the features described above, include on-line, e-journals where an established refereeing procedure is used and off-line, refereed, electronic media such as the CD-ROM. The later has the advantage of being independent web access (but using many of the web software tools) and capable of being archived in a permanent form independent of a specific host computer(s).

In reviewing the development of image processing in fluid mechanics material available on the web the highly variable quality of both content and presentation, together with absence of timely revision, in many cases, made it unsuitable for the present purpose. In order to combine recent refereed publication with an international flavour the author has conducted a full text search of the recent electronic proceedings of the 8th International Symposium on Flow Visualization [2] using sample keywords frequently found in image processing. In this way a high quality sample of images and digital movies was identified and will be presented at the symposium. The advantages of the electronic media will be further utilised using new developments in image compression and animation for inclusion in the electronic proceedings of the 9th International Symposium on Flow Visualization [3].

SAMPLE KEYWORDS AND REPRESENTATIVE EXAMPLES

Colour (118 papers)

The availability of inexpensive colour CCD technology has lead to the use of multi-line lasers, and occasionally, white light as a means of illumination. The colour components of the light source are then used to isolate particular features in the experiment. These include slopes of water waves, time of exposure in multi-exposure visualisation or object tracking, combustion conditions, temperature or pressure using sensitive crystals, three colour differential geometry and coloured Schlieren.

Correlation (111 papers)

The use of correlation techniques in flow image processing has played an important part in the development of particle image velocimetry. Both digital and analogue hardware systems have been developed to facilitate efficient calculation. Commonly both auto correlation (single image, multiple exposure) and cross correlation (multiple images, single exposure) are being used, the latter giving an implicit measure of time and therefore flow direction. The method is particularly used in images of high feature density. Recently, cascade methods have been used where local correlation function measurements are used to aid subsequent image grouping.

Image Filtering (102 papers)

The images produced in flow visualisation are frequently subjected to filtering both to isolate coloured features and region of common wave number. In addition image restoration or improvement is often achieved using sharpening, edge detection and a variety of particular transforms for specialist requirements, spatial filtering of velocity components to identify flow structures.

Smoothing (75 papers)

Common smoothing procedures apply a low pass filter to image data in a variety of methods. Local weighted pixel averaging, such as median or hysterisis methods, are examples.

Transform (72 papers)

The use of transformation methods is a common and is a powerful technique used in image improvement and analysis. Common transformation methods include the Fourier transform, Abel inverse transform and wavelet transform.

Histogram (16 papers)

The use of histogram analysis on the pixel array of an electronic image allows rapid sorting of significant data on the basis of intensity or feature grouping. It is the basis of many feature-tracking procedures where multiple body, or flow structure, behavior is being investigated. In this context it is used as a first step in a cascade process where a higher accuracy is finally obtained by multi-step processing.

Sub-pixel resolution (15)

The quantisation effect produced by the sampling of an image by discrete pixel elements presents many classical problems in ambiguity. The increased resolution produced by curve fitting of intensity values within local pixel groups.

Binarisation (10 papers)

In extraction of particle images from a low contrast image, a level of brightness is chosen as a threshold for binarisation of the image. By choosing pixels above the brightness threshold out-of-focus particles and background effects are eliminated.

Stereo (9 papers)

At present many laboratories are developing three component velocity measurement systems which extract the out of plane velocity component using multiple views of the same scene. The efforts have recently concentrated both in improving the optical viewing arrangements and simplifying the arduous calibration procedure.

Neural methods (5 papers)

Computational procedures have been developed which use a conceptual model of the human brain as an inspiration for digital algorithm development. The brain is essentially a massive parallel processing system with links between the processors being varied by brain chemistry and in this way controlling the thought, or computational, processes. Examples of the method applied to piv include multi-layer adaptive filtering and stereo image matching using an optimization network.

Edge detection (4 papers)

This is useful in multi-phase flows where component boundaries need to be established in order to measure the phase fractions and the velocities of individual phase components. Examples include bubbles in a sediment carrying liquid and flames.

LIST OF EXAMPLE SEARCH ENGINES / DATA BASES

Alta Vista, Alta Vista Canada, Anzwers, AOL Net Find, Canada.com, Euroseek, Excite, Google, GoTo.com, HotBot, InfoHiway, InfoSeek, Magellan, Northern Light, Snap, UKMax, Web Crawler, What-U-Seek, Yahoo (USA).

REFERENCES

1. Gonzalez, R. C. and Wintz, P.: Digital Image Processing, Addison-Wesley Publishing Company, 1977

2. Proceedings of the 8th International Symposium on Flow Visualization, Editors G M Carlomagno and I Grant. *On* CD Rom ISBN 0 9533991 0 9. (http://www.ode-web.demon.co.uk/post-conf-web/flyer.html) Sorrento, Italy, September 1-4, 1998

3. Proceedings of the 9th International Symposium on Flow Visualization, Editors G M Carlomagno and I Grant. *To be published On* CD Rom. (http://www.ode-web.demon.co.uk/9misfv/) Heriot-Watt University, Edinburgh, Scotland, UK. August, 22-25, 2000.

DIGITAL HOLOGRAPHY AND HOLOGRAPHIC INTERFEROMETRY

Thomas M. Kreis

BIAS - Bremer Institut für angewandte Strahltechnik
Klagenfurter Str. 2, D 28359 Bremen, Germany

Summary In digital holography optically generated Fresnel- or Fraunhofer holograms are recorded by a CCD array. The reconstructed wavefields are computed by multiplication of the digital hologram with a numerical model of the reference wave and solution of the diffraction integral. This can be done by the Fresnel transform or by employing the convolution theorem. Both approaches result in a complex field from which intensity and phase can be determined. The sign-correct interference phase in digital holographic interferometry is computed with high accuracy by subtraction of two such phase distributions.

CCD recording of digital holograms

Holographic interferometry is a prominent tool for high-precision measurement of deformation fields at opaque surfaces of mechanical components. From the evaluated deformation vector fields strains and stresses can be calculated. But up to now the holograms had to be developed in a wet-chemical process. Thermoplastics or photorefractive crystals also have their specific drawbacks. The holograms must be replaced exactly into the holographic arrangement. For high-precision sign-correct results several phase shifted interferograms had to be reconstructed, recorded and stored in computer. Then from the reconstructed intensities the interference phase distribution had to be determined by suitable algorithms[1].

In digital holography Fresnel or Fraunhofer holograms are recorded by a CCD array and the complex wavefields are reconstructed numerically. Digital CCD-recording of holograms is possible as long as the sampling theorem is fulfilled. This demands that each period of the spatial variation in the hologram intensity is sampled by at least two pixels of the CCD array. Therefore the angle between object wave and reference wave must remain small. The largest admissible angle is dictated mainly by the size of the CCD pixels. A small angle is obtained by objects with small lateral dimensions, or by objects placed far from the CCD array, or by optical reduction of a large object and the recording the small virtual image of this object[2].

Any reference wave can be used as long as the sampling theorem is fulfilled: collimated or divergent, normally or obliquely impinging onto the CCD array[3]. The recommended reference wave is the plane wave falling normally onto the CCD because it yields small angles and is easy to handle numerically because it is modeled by only a real constant.

Numerical reconstruction of digital holograms

Physical holograms are reconstructed by illumination with the reference wave. But now the digital holograms stored in computer are reconstructed by multiplication with a numerical representation of the reference wave field and calculation of the resulting diffraction field in the image plane, Fig. 1. This field is given by the diffraction integral

$$b'(x',y') = \frac{1}{i\lambda}\int\int h(\xi,\eta)r(\xi,\eta)\frac{\exp\{ik\rho\}}{\rho}d\xi\,d\eta \qquad (1)$$

with $\rho = \sqrt{d'^2 + (\xi - x')^2 + (\eta - y')^2}$. $h(\xi,\eta)$ is the recorded hologram, $r(\xi,\eta)$ represents the reference wave field, $k = 2\pi/\lambda$ denotes the wave number[4]. For the normally impinging plane reference wave $r(\xi,\eta)$ is constant and can be omitted[5].

If the distance d between object and hologram plane, and equivelantly $d' = d$ between hologram and image plane, is large compared to $(\xi - x')$ and $(\eta - y')$, then the ρ in the denominator under

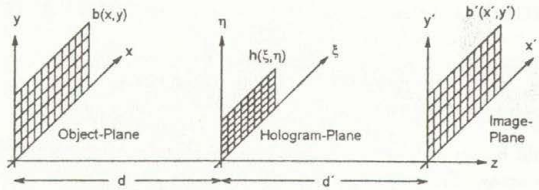

Figure 1: Geometry of digital Fresnel holography

the integral of (1) can be replaced by d'. For the ρ in the exponential of the numerator we can use the binomial expansion $\sqrt{1+a} = 1 + \frac{1}{2}a - \frac{1}{8}a^2 + - \ldots$ with $a = (\xi - x')^2/d'^2 + (\eta - y')^2/d'^2$. Taking only the constant and the linear terms of this series, the diffraction integral becomes

$$b'(\nu,\mu) = A \int\int h(\xi,\eta) r(\xi,\eta) \mathrm{e}^{\frac{i\pi}{d'\lambda}(\xi^2+\eta^2)} \mathrm{e}^{-2i\pi(\xi\nu+\eta\mu)} d\xi \; d\eta \tag{2}$$

with $A = \frac{\exp\{ikd'\}\exp\{i\pi d'\lambda(\nu^2+\mu^2)\}}{i\lambda d'}$, $\nu = x'/(d'\lambda)$ and $\mu = y'/(d'\lambda)$. Up to a factor which does not depend on the evaluated hologram, the diffracted field is the Fourier transform of the hologram $h(\xi,\eta)$ multiplied with the reference wave $r(\xi,\eta)$ and the chirp function $\exp\{i\pi(\xi^2+\eta^2)/(\lambda d')\}$. The stored digital hologram consists of $N \times M$ discrete values, each recorded by a pixel of size $\Delta\xi \times \Delta\eta$. The finite discrete Fresnel transform now is

$$b'(n,m) = \mathrm{e}^{i\pi d'\lambda\left(\frac{n^2}{N^2\Delta\xi^2} + \frac{m^2}{M^2\Delta\eta^2}\right)} \sum_{k=0}^{N-1}\sum_{l=0}^{M-1} h(k\Delta\xi, l\Delta\eta) r(k\Delta\xi, l\Delta\eta) \mathrm{e}^{\frac{i\pi}{d'\lambda}(k^2\Delta\xi^2 + l^2\Delta\eta^2)} \mathrm{e}^{2i\pi\left(\frac{kn}{N} + \frac{lm}{M}\right)} \tag{3}$$

where the constant factor $\exp\{ikd'\}/(i\lambda d')$ has been omitted for clarity.

A second approach to the determination of $b'(n,m)$ uses the convolution theorem. The diffraction integral (1) represents a linear shift-invariant system and thus is a convolution. Now $b'(x',y')$ is calculated by $b' = \mathcal{F}^{-1}\{\mathcal{F}\{h \cdot r\} \cdot \mathcal{F}\{g\}\}$, which is the inverse Fourier transform of the product of the Fourier transforms of $h \cdot r$ and the impulse response g. The finite discrete realization of the impulse response for free space propagation is

$$g(k,l) = \frac{\exp\left\{\frac{2i\pi}{\lambda}\sqrt{d'^2 + (k-N/2)^2\Delta\xi^2 + (l-M/2)^2\Delta\eta^2}\right\}}{i\lambda\sqrt{d'^2 + (k-N/2)^2\Delta\xi^2 + (l-M/2)^2\Delta\eta^2}} \tag{4}$$

The coordinate shifts by $N/2$ and $M/2$ are on symmetry reasons. Alternatively we can define the transfer function G, which is the Fourier transform of g, directly, thus saving one Fourier transform $b' = \mathcal{F}^{-1}\{\mathcal{F}\{h \cdot r\} \cdot G\}$, or we may employ the Fresnel approximations[3,6] of g or G.

Fresnel transform (3) as well as convolution reconstruction yield complex wave fields $b'(n,m)$. From them intensity and phase distributions can be calculated by

$$I(n,m) = b'(n,m) \cdot b'^*(n,m) \qquad \text{and} \qquad \phi(n,m) = \arctan\frac{\mathrm{Im}[b'(n,m)]}{\mathrm{Re}[b'(n,m)]} \tag{5}$$

A difference in the two reconstruction concepts is that the result of the Fresnel transform is in the spatial frequency domain. Therefore the pixels represent spatial frequencies and have a pixel spacing, or equivalently pixel size, in the reconstructed field

$$\Delta x' = \frac{d'\lambda}{N\Delta\xi} \qquad \Delta y' = \frac{d'\lambda}{M\Delta\eta} \tag{6}$$

On the other hand the result of the convolution is again in the spatial domain. So the pixel size in the reconstructed image now is $\Delta x' = \Delta\xi$ and $\Delta y' = \Delta\eta$. Here the pixel size does not depend on d' or λ, as in the Fresnel case. The often annoying bright rectangular or square dc-term in digital holography can be eliminated numerically by applying a proper digital highpass filter to the digital hologram[7].

Digital holographic interferometry

In digital holography we have access to the individual phase distributions of the wave fields according to the two deformation states, so the modulo 2π interference phase $\Delta\phi(n,m)$ can be determined by subtracting the two reconstructed phase distributions[8]. An efficient way to perform this modulo subtraction is by

$$\Delta\phi(n,m) = \arctan \frac{\mathrm{Re}\{b'_1(n,m)\}\mathrm{Im}\{b'_2(n,m)\} - \mathrm{Re}\{b'_2(n,m)\}\mathrm{Im}\{b'_1(n,m)\}}{\mathrm{Re}\{b'_1(n,m)\}\mathrm{Re}\{b'_2(n,m)\} + \mathrm{Im}\{b'_1(n,m)\}\mathrm{Im}\{b'_2(n,m)\}} \tag{7}$$

There is no intensity involved which destroys the sign due to $\cos(-\phi) = \cos\phi$, so the interference phase in digital holographic interferometry is sign-correct.

As an example a rectangular plate of about $12cm \times 8cm$ was centrally pressed from the rear side after taking the first digital hologram and then the second hologram was recorded. Before the third recording the plate was shifted horizonally. The reduced virtual image of the plate was a distance $d' = 0.254m$ away from the CCD array of $N \times M = 1024 \times 1024$ pixels of size $\Delta\xi = \Delta\eta = 6.8\mu m$. Wavelength was $\lambda = 0.6328\mu m$, the reference wave was a normally impinging plane wave. In Fig. 2 we see the interference phases modulo 2π of the comparisons of the first and the second (left picture), the second and the third (central), as well as the first and the third hologram (right).

Figure 2: Interference phase distributions

Having now numerical access to the interference phase, one may attempt to compensate motion components which lead to high fringe densities by adding or subtracting artificial phase distributions. Although we will get no additional information by this procedure, sometimes fine details in the display of the interference phase distribution are better recognizable. The left display of Fig. 3 shows the same phase as the central picture in Fig. 2, but now a linear phase that increased from 0. rad at the left edge to 150 rad $\approx 24 * 2\pi$ at the right edge was subtracted. The display at the right shows the same measured phase difference as given in the center, but a phase increasing linearly by 300 rad $\approx 48 * 2\pi$ was subtracted.

Digital holographic interferometry also is used advantageously for contour measurement. Fig. 4 gives three examples of holographic contouring of a plane surface with a central spherical cap.

Figure 3: Compensation of motion components by subtraction of linearly varying phases

The left picture gives the phase after shifting the illumination point between the recordings of the digital holograms, the central picture comes from a change of the wavelength, and the right one was produced by varying the refractive index of the liquid the object was immersed in.

Figure 4: Modulo 2π contours after shifting the illumination points, varying the wavelength, and changing the refractive index of the surrounding medium

Acknowledgement

The described fundamental research was sponsored by the German Research Council (Deutsche Forschungsgemeinschaft DFG) under grant Kr 953/12-2 which is gratefully acknowledged.

References

1. Th. Kreis: Holographic Interferometry: Principles and Methods, Akademie-Verlag, Berlin, and VCH Publishers, Inc., New York, 1996.

2. U. Schnars, Th. M. Kreis, and W. P. O. Jüptner: Digital recording and numerical reconstruction of holograms: reduction of the spatial frequency spectrum. *Opt. Eng.*, 35(4), 977–982, 1996.

3. Th. Kreis, M. Adams, and W. Jüptner: Methods of Digital Holography: A Comparison. *Conf. on Optical Inspection and Micromeas. II*, Proc. SPIE vol. 3098, 224–233, 1997.

4. J. W. Goodman: Introduction to Fourier Optics, McGraw-Hill Inc., New York, 2nd Edit., 1996.

5. U. Schnars: Direct phase determination in hologram interferometry with use of digitally recorded holograms. *J. Opt. Soc. Amer. A*, 11, 2011–2015, 1994.

6. Th. Kreis and W. Jüptner: Principles of digital holography. *Proc. of Fringe 97, 3rd Intern. Workshop on Automatic Processing of Fringe Patterns*, 353–363, 1997.

7. Th. Kreis and W. Jüptner: The suppression of the d.c.-term in digital holography. *Opt. Eng.*, 36, 2357–2360, 1997.

8. Th. Kreis, W. Jüptner, and J. Geldmacher: Principles of Digital Holographic Interferometry. Laser Interferometry IX: Techniques and Analysis, Proc. SPIE vol. 3478, 45–54, 1998.

PHASE METHODS OF FRINGE PATTERN ANALYSIS

Małgorzata Kujawińska
Institute of Micromechanics and Photonics, Warsaw University of Technology
8 Chodkiewicza St., PL 02-525 Warsaw, Poland

Summary The recent success in implementation of optical full-field measuring methods into research, industrial, medical and commercial areas depends on automatic analysis of their output e.g. fringe patterns, FP. The demands of recent systems are to retrieve a measurand coded in fringe pattern faster, more accurate and reliable. The paper is intended to be a review of fringe pattern analysis methods, FPA, and their capabilities to analyse an extended class of images. The special emphasis is paid to phase methods which require to design of FP features such as temporal and spatial carrier frequency or phase shifts. The main trends in development of phase methods and algorithms together with comparison of their capabilities are presented. The methods are illustrated by numerous examples of fringe pattern analysis in shape, displacement and deformation measuring systems.

Introduction

Optical methods of testing with the output in the form of interferogram, or more general fringe pattern, have been used since early 1800s. However the routine quantitative interpretation of the information coded into fringe pattern was not practical in the absence of computers. In the late 1970s the advances in video camera and image processing and computer technology provided the means for the birth and rapid development of automatic fringe pattern analysis.

In general fringe pattern analysis refers to full reconversion of the original feature (or features) represented by a fringe pattern. In simplified version it can be viewed as technique for conversion of sinusoidal intensity fluctuation in space:

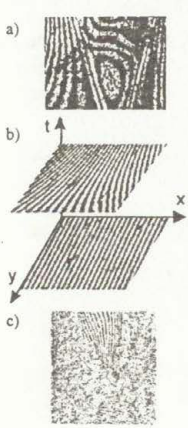

$$I(x,y) = a(x,y) + b(x,y) \cos \phi\,(x,y) \qquad (1)$$

where a(x,y), b(x,y), are background and local contrast, respectively and ϕ (x,y) is the phase function obtained when an interferometer, moiré system or other devices produces a continuous map which is an analogue of the physical quantity being measured (shape, displacement, deformation, strain, temperature, etc.).

This definition leads to the main problem in fringe analysis when we measure intensities I(x,y), but have to compute phase ϕ, we have to solve an inverse problem with its all difficulties:

- the regularization problem (ill posed problem due to the presence of unknown a(x,y), b(x,y) and ϕ(x,y))
- the sign ambiguity problem ($\cos(\phi) = \cos(-\phi)$)
- the mod 2π problem ($\cos(\phi) = \cos(\phi+2N\pi)$)

Fig. 1. The various classes of fringe patterns rep-resenting: a) static objects with noise, b) variable in time objects and c) multiplexed objects

Additional difficulties are introduced by the white or coherent noise and the presence of higher harmonics in the intensity signal (Fig. 1a)

$$I(x,y)=a_0(x,y)+\sum_{n=1}^{\infty}b_n(x,y)\cos[n\phi(x,y)]+n(x,y) \tag{2}$$

as well as the fluctuatiary of the intensity in time (Fig. 2b) which occurs in the case of dynamic event or the measurements in nonstable environment:

$$I(x,y;t)=a_0(x,y;t)+\sum_{n=1}^{\infty}b_n(x,y;t)\cos[n\phi(x,y;t)]+n(x,y;t) \tag{3}$$

In the case of more complicated measuring tasks interferograms may contain multiplexed information about two or more measurands (Fig. 1c).

$$I(x,y)=\left(\sum_{k=1}^{K}\text{lub}\bigcap_{k=1}^{K}\right)\left\{a_{0k}(x,y)+\sum_{n=1}^{\infty}b_{nk}(x,y)\cos[n\phi_k(x,y)]\right\}+n(x,y) \tag{4}$$

Due to extended range of fringe patterns and multiplicity of the measurement tasks several techniques for automatic and precision reconstruction of phases from fringe patterns were developed. Below we present the description and analysis of the applicability and trends in development of these methods.

Overview of fringe pattern analysis process

From historical reasons the fringe pattern analysis methods may be divided into two groups (Fig. 2).

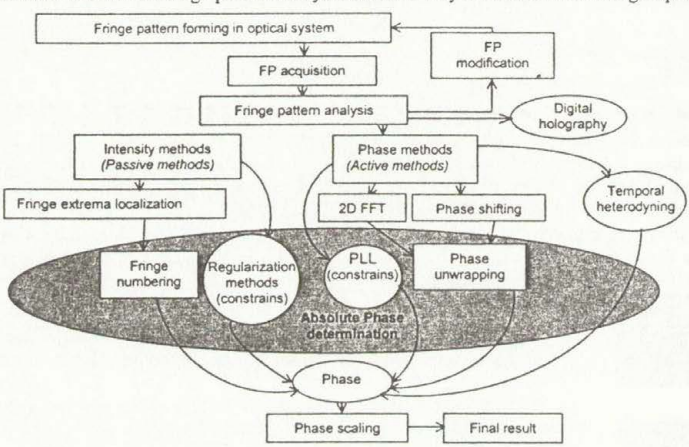

Fig. 2. The general scheme of fringe pattern analysis process

During last 20 years several techniques for the automatic and precision reconstruction of phases from fringe patterns were developed[1]. From historical reasons they may be divided into two groups (Fig. 1):

- **intensity methods** which can be also named **passive methods**, as we analyse a fringe pattern without its modifications and in order to solve the first two ambiguities, we have to relay on a priori knowledge or allow certain restrictions.
  Passive methods include: fringe extrema localization techniques (skeletoning, fringe tracking), which are based on conventional image processing algorithms and newly developed regularization methods which solve the inverse problem by integrating prior information about the physical variable in order to obtain a unique and plausible solution,
- **phase methods** which can be also named **active methods**, as we actively modify the phase of the fringe pattern, which is represented by the equation:

$$I(x,y;t) = a(x,y) + b(x,y)\cos[\phi(x,y) + 2\pi(f_{0x}x + f_{0y}y + \nu_0 t) + \alpha(t)] \quad (5)$$

where f_{0x}, f_{0y} are the fundamental spatial frequencies, ν_0 is the fundamental temporal frequency and α is the phase shift value.

The phase modifications provide additional information to solve the regularization and sign ambiguity problem by means of the following phase measuring methods:

- temporal heterodyning (introducing ν_0), this is electronic hardware based method. It detects the beat frequency of a signal created by the superposition of two slightly frequency shifted signal and measures the phase ϕ, but ϕ mod (2π). We predict that with the technology progress of the CCD detectors with the separate parallel and specialized outputs from each pixel, the temporal heterodyning may become the leading technique for accurate, real-time phase detection,
- spatial heterodyning (introducing f_{0x}, f_{0y}) including: Fourier transform method, Phase-locked loop, PLL and spatial carrier phase shifting method,
- temporal and spatial phase shifting (introducing α), which are discrete versions of the above methods, where the time or spatially varying interferograms is sampled over a single period.

Recently in addition to the passive and active fringe pattern analysis methods (see Fig. 1) the new possibility appears at the "phase measuring market", namely **digital holography**[2]. Digital holography gives numerical access to the whole optical field, amplitude and phase, therefore the information, previously coded into fringe pattern, can be calculated by simple subtraction of the object's phases before and after its changes. This approach is at the moment computational extensive and requires very high spatial resolution of the CCD detectors. However due to its generality and high information content it may become in future competitive towards recently used methods.

Due to the sinusoidal nature of the signal, most of the fringe pattern analysis methods deliver the phase with 2π ambiguity i.e. in the from of so called "phase fringes", which require solving of absolute phase problem[3]. This is approached by:

- application of additional means (knowledge),
- modification of system parameters

and uses one of the following method:

- fringe numbering and phase extrapolation,
- regularized phase tracking techniques,
- phase unwrapping and hierarchical unwrapping.

Absolute phase determination finalizes the fringe pattern analysis process, which reduce a fringe pattern to a continuous phase map. However to solve a particular engineering problem, the phase scaling has to be implemented. It converts the phase map into the physical quality to be measured in the form which enables further information processing and implementation in CAD/CAM and FEM packages, industrial control and other measurement systems. This last stage is out of scope of this paper although often it is an integral part of commercial fringe pattern analysis system.

Trends in development of phase measuring methods

Modern fringe pattern analysis systems should enable to retrieve a measurand coded in a fringe pattern automatically, fast, accurate and reliable. The choice of the method applied depends on many environmental, hardware and software conditions and measurement requirements (accuracy, speed), as well as on the class of fringe patterns often with high noise, closed fringes, physical discontinuities, containing complex information about several objects or phenomena which are static or dynamic.
The methods most often used in modern commercial systems are:

- temporal phase shifting TPS: method applied for high accuracy measurement of static objects. The basic idea of TPS is to obtain n fringe patterns with a constant phase increment $\alpha(t)$ between two consequtive frames, so that a given pixel is sampling a periodic intensity waveform over one period,
- spatial carrier phase shifting method, SCPS; method for medium accuracy industrial measurements and analysis of dynamic phenomena. In SCPS the spatial carrier fringes (e.g. f_{ox}) are introduced into a fringe pattern, so that a waveform period is sampled over adjacent pixels.

It has been recognized in both methods that errors can be introduced to phase evaluations if the fringe pattern is not a perfect sine and if the phase shift is different from its nominal value. A number of algorithms have been proposed to deal with either or both causes in specific cases. However the most interesting and general method uses the Fourier approach developed by Freischlad and Koliopoulos[4].
In general, the Fourier-transform approach shows that the minimal number of intensity values required to obtain insensitivity up to the jth order, to the harmonic content of the signal in the presence of a constant phase shift miscalibration is $2j + 2$ and the phase shift has to be $2\pi/(2j+2)$ between the temporal (TPS) or spatial (SCPS) samples. However if SCPS method is used for highly distorted fringes the algorithms has to be additionally modified (due to strong violation of the condition of constant phase values in the neighborhood of the actual pixel). In such cases SCPS method with the assumption of constant phase gradient should be applied.

The knowledge about the relationship between a fringe pattern and the output accuracy of the phase retrieved by a chosen algorithm is the basis for a smart optical measurement system shown in Fig. 3. The philosophy of the system[5] includes active fringe pattern modification active and adaptive algorithm design supporting each other in order to provide the reconstruction of hardware settings important from the algorithm point of view and provide the data to adapt the parameters of the algorithm.
The other recent tendency in fringe pattern analysis methods is to form hybrid methods which combine advantages of the well known approaches including:

- spatial and temporal heterodyning[6]. The spatio-temporal approach may be used for analysis of multiple objects and moving or variable in time objects,
- single point and neighbourhood based analysis[7]. This approach combines phase-shifting and regularized phase tracking methods. It determines a suitable spatial-temporal phase estimator which takes into account not only one pixel of the phase shifted interferograms but rather a small neighbourhood around it. This additional information leads to significant improvement in the signal to

noise ratio of the recovered phase and high improvement in the harmonic rejection of the light detector used.

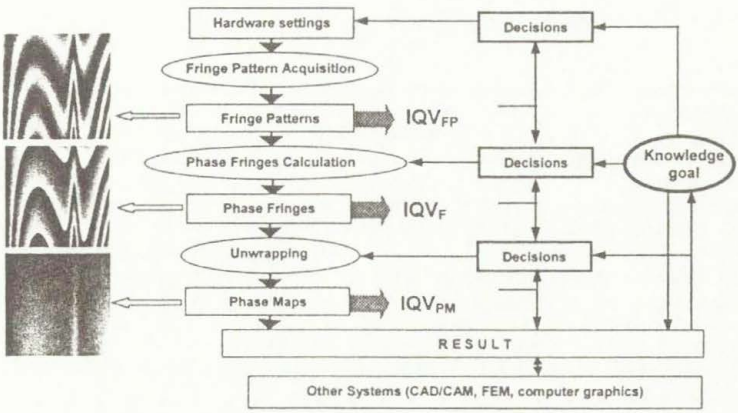

Fig. 3. Adaptive fringe pattern analysis: IQF_{FP}, IQV_F, IQV_{PM} – the image quality vectors for fringe pattern, phase fringes and phase map, respectively

The above summary shows that after thirty years of extensive works on automatic fringe pattern analysis still a lot of scientists work on development of new approaches and improvement of the widely used methods. The reason for this is simple, the success in implementation of optical full-field measuring methods into industrial, medical and commercial areas depends on proper retrieving of a measurand coded in an arbitrary fringe pattern. It should be done fast, automatically, accurately and deliver the output data in a form compatible with other systems (CAD/CAM, FEM etc.). In order to fulfil these requirements for wide class of objects or phenomena analysed, the new solutions in phase measuring methods focus on the following issues mentioned in the paper:

- active approach to fringe pattern forming (through the concept of smart phase measuring system),
- active approach to phase shifting algorithm design (through Fourier descriptors),
- forming hybrid methods of fringe pattern analysis based on spatio-temporal concept.

Additional "hot" topics include exploring the capabilities of digital holography and introducing concepts of absolute phase measuring methods which are discussed in two other keynote lectures during Euromech 406 Conference.

References

1. D.W. Robinson, G.T. Reid (eds), "Interferogram Analysis: Digital Fringe Pattern Measurement Techniques", Institute of Physics Publ., Bristol and Philadelphia, 1993
2. U. Schnars, "Direct phase determination in hologram interferometer with use of digitally recorded holograms", J.Opt.Soc.Am.A, v. 11, 2011-2015, 1994
3. W. Osten, W. Nadeborn, P. Andra, "General hierarchical approach in absolute phase measurement", Proc. SPIE, v. 2860, 2-13, 1996
4. K. Freischlad, C.L. Koliopoulos, "Fourier description of digital phase-measuring interferometer", J.Opt.Soc.Am. A, v. 7, 542-551, 1990
5. M. Kujawińska, C. Kosiński: "Adaptability: Problem or Solution" in Akademie Verlag Series in Optical Metrology, W.Jüptner, W.Osten (Eds) Akademie Verlag Series in Optical Metrology, v. 3, 419-431, 1997
6. M. Takeda, M., Kitoh, "Spatio-temporal frequency-multiplex heterodyne interferometer", JOSA A, v. 9, 1607-1614, 1992
7. M. Servin, R. Rodriguez-Vera, J.L. Marroquin, D.Malacara, "Phase shifting interferometer using a two-dimensional regularized phase tracking (RPT) technique", Journal of Modern Optics, 1997

ACTIVE VISION IN OPTICAL METROLOGY

Wolfgang Osten

Bremer Institut für Angewandte Strahltechnik, Klagenfurter Str. 2, D-28359 Bremen
e-mail: wolfgang@alf.zfn.uni-bremen.de

For some years a new way of thinking appears with respect to the solution of vision tasks. A paradigm has already arisen, known under the various names *Active/Purposive/Animate*, etc. - *Vision.* There is an important difference between the active and the classic *passive* as well as *adaptive* approach. When we work in passive mode, a set of images is given which have to be processed with the algorithms we are going to develop. On the other hand, when we work in active mode we do not want prerecorded data since we include the image acquisition as an component of equal importance into the complete evaluation process. And this means far more than making the system adaptive to unfavourable boundary conditions such as a shading correction at unevenly illuminated scene.

Active vision offers a new approach for building intelligent and more flexible systems. In this sense an active system is not only able as just to „see". It is designed to do something, i.e. to make an action, which is anything that changes the state of the system or the environment. Similar to human perception as an active way to explore a natural scene by changing the view or the focus, the role of the observer and observation system, respectively, is defined as an active component for gathering data. Further on the strategy for solving an image analysis problem is actively influenced by use of controlled feedback loops between the components that capture the optical information and those that evaluate it.

In computer vision and optical metrology sometimes the difference between a so called active and passive technique is only made with respect to the way of working with the light, i.e. illumination. For instance in shape measurement the technique *shape from shading* is classified as an passive technique whereas *structured light illumination* is called as active. The difference between both approaches is that in the first case the shape is recovered from the brightness at each point of an image usually illuminated by one point light source with the same lighting throughout the surface and in the second case the structure of the lighting is modulated systematically throughout the surface of the object. In my understanding the other way of object illumination by using structured light delivers not more as the possibility to realize the triangulation principle in a fieldwise manner by addressing each point with a mod 2π phase value. But a lot of problems still remain, especially with respect to the ambiguity of the phase reconstruction. Here the application of more sophisticated procedures such as *absolute phase measurement* or *wavelength scanning* is necessary with respect to a unique solution. These methods bring a certain amount of activity into the system since the role of the observer is active by capturing more information as a single view can bring. However, active vision/metrology is not just the use of multiple frames. The modern understanding of being active means that the image acquisition process is controlled and thus constraints that facilitate the recovery of information about the state of the object under test (3D shape, 3D displacement, subsurface defects, ...) are introduced. The contribution describes the origin of the problems and why only an active approach can be successful in many measurement problems. To explain the different ways of dealing with problems in optical metrology a well known example is used that is quite common for a lot of applications namely the reconstruction of continuous phase distributions from 2D fringe patterns.

DIFFERENTIAL INTERFEROMETRY OR „SHEAROGRAPHY": USE IN FLUID MECHANICS AND IN SOLID MECHANICS. A LONG STORY.

P. Smigielski – French German Research Institute
68300 Saint-Louis - France

Summary :

Differential interferometry in polarized light using Wollaston prisms is a wellknown technique used for a very long time for flow visualization either with white light or with a laser source. „Shearography" was used more recently but in solid mechanics mainly for non-destructive testing. A laser source is necessary with this technique. This paper will describe different set-up and applications in both fields of mechanics and will comment upon sensitivity, spatial and temporal coherence, and image processing. An outlook on the future will be done including new developments on digital interferometry.

1. Generalities :

For several years speckle interferometry systems have been used more and more in solid mechanics to measure the displacements at each point of a solid diffusing object submitted to different stress and strains :
- TV-holography systems (or ESPI : Electronic Speckle Pattern Interferometers)which measure out-of-plane displacements are mainly used for vibration analysis.
- speckle interferometers with two symetrical illuminating beam which are able to measure in-plane displacements are used for strain analysis;
- shearography systems which are differential interferometers are mainly used for non-destructive testing.

For a more long time, interferometers and differential interferometers have been used in fluid mechanics.

The most important difference between interferometers used in solid mechanics and in fluid mechanics concerns the type of objects studied. In solid mechanics we generally studied solid objects which diffuse the light illuminating them while in fluid mechanics objects are generally transparent to light. When a laser is used as a light source, solid diffusing objects generate an interference pattern called „speckle" which is a coherent noise. For that reason, the term speckle interferometer is not well appropriate from my point of view. A speckle interferometer is a classical interferometer with a strong noise due to the „roughness" of the object. With transparent objects as those met in fluid mechanics, there is generally no speckle. That means that optical systems or image processing used in both cases can be almost identical !

To illustrate what we say, we will take as a good example the case of shearography or differential interferometry (as you like depending of your field of activities !). Researchers and engineers working in the field of solid mechanics and no specialists of optics could have the feeling that shearography is a new method.When it is in fact a very old method well-known by the people working in the field of fluid mechanics as differential interferometry but relatively recently well adapted by opticians to objects diffusing coherent light and therefore generating a speckle.

2. Diffential interferometry

In classical interferometers as Michelson interferometers or Mach-Zehnder interferometers the two interfering beams are totally separated and only one beam passes through the transparent object (fluid mechanics applications) or is diffusely reflected by the solid object (solid mechanics applications). That means strong vibrational or thermal sensitivity and leads to some adjustment difficulties.In addition, the measurement sensitivity is not variable.
In differential interferometry, the two light beams have only a very small displacement to each other the („shearing"), which greatly reduces the undesirable sensitivity (vibrations, thermal effects, ...) and makes the optical adjustments more easy and the use of an incoherent light source possible. The sensitivity is easily variable by simply changing the value of the displacement (the shearing) between the two interfering light beams.
Due to the fact that the two beams are almost superimposed, they pass together through the phase object or are together reflected by the solid object. Therefore the method leads to a differential measurement (approximatively the first spatial derivative of the optical path in the direction of the shearing).
Among the great variety of optical means that may be used for beam separations (or to create the shearing !), I shall report on two systems : the Wollaston prism and the Michelson interferometer.

2.1 Use of a Wollaston prism in polarized light

Wollaston prisms were originally developed for use in interference microscopes [1]. Their application has been extended since 1954 to flow diagnostics [2].[3]
They can be used either with white light or with coherent light (laser).

a) use with a white light source

Figure 1 shows a typical optical arrangement used at ISL for supersonic or hypersonic flow studies [3].
A light-ray coming from a point of an incoherent source (typically a spark gap) is symetrically split by a Wollaston prism into two light rays of perpendicular polarization having an angle ε between them.
If the original ray coming from the point source is linearly polarized under 45° (with a polarizer) relatively to the optical axes of the prism, the two output beams have the same intensity. The Wollaston prims being situated at the object focal point of an achromatic lens, the two output light rays run parallel to the optical axis of the optical system with a separation distance $e = f.\varepsilon$, f being the focal lenght of the lens.
After having passed through the transparent phase object (aerodynamic phenomenon), the two light rays are superimposed with a second Wollaston prism correctly oriented. Because of their perpenticular linear polarization, they can only interfere after being polarized (with a polarizer) in a common direction (preferentially 45 °).
If the two Wollaston prisms are exactly placed in the focal planes of the two lenses (see picture), the interferometer imparts the same optical path difference to all the double rays arriving on the detector (photographic plate or CCD camera) and the interferogram (with no phase object) shows no fringe : the fringe spacing is the infinite. When the prisms are moved along the optical axis, then parallel and equidistant fringes appear in the direction which is normal to the beam separation.
Some examples of differential interferograms are shown figure 2 in order to give an idea of the possibilities of the method.[4]

b) Use with a laser

Instead of using a white light source allowing to get color fringes and some possibilities to obtain the absolute value of the optical path, by the Newton color chart [5], it is possible to use a pulse laser to have more contrasted monochromatic interference fringes [5] (figure 3). For quantitative results in this case we can use Fourier transforms as thas is done with shearography in solid mechanics.
Obviously, we get only the optical path integrated through the transparent object. To get the refractive index value (or the specific mass associated with the Gladstone law) in a point of the object in a 3D-flow (general case) we have to use tomography i.e we have to get N interferograms recorded in N different directions. In some cases (axi-symetrical or 2D-flows) only one interferogram is necessary.
Remark : Using a double exposure technique you have a possibility to get quantitative results.
The interference fringes can be described by the intensity I

$$I = Io\ (1 + m \cos \delta\varphi)$$

Io being the intensity of the background, m the contrast of the fringes, and $\delta\varphi$ the optical phase difference between two correlated light rays separated in the object field by the distance e (the shearing).
As in a shearography technique, we have 3 unknowns and we need 3 or more equations to get $\delta\varphi$. It is relatively easy to get m = 1. By playing with the polarization of the light, it is possible to obtain two equations

$$I_1 = Io\ (1 + \cos \delta\varphi) \text{ and } I_2 = Io\ (1 - \cos \delta\varphi) \text{ and to get } \cos \delta\varphi = (I_1 - I_2) / (I_1 + I_2)$$

2.2 Use of a Michelson interferometer

Here, the shearing is obtained by using a Michelson interferometer in coherent light (with a laser) with adapted optics on the beam reflected by the solid object under testing or transmitted through the phase object under investigation.[figure 4]
By tilting of a mirror of the interferometer you can easily change the shearing.

a) use in solid mechanics

The main application concerns industrial non destructive testing. The quasi-static object under investigation is submitted to a strain (pressure or temperature stressing, ...) allowing a defect inside the object to be represented by a small deformation at the surface of the object illuminated by a laser beam. The goal is to visualize this small deformation.
Before stressing, we have a reference picture described by its intensity I_R :

$$I_R = Io\ (1 + m \cos \Delta\varphi_R)$$

with $\Delta\varphi_R = \varphi_2 - \varphi_1$, the phase difference due to the shearing.
After stressing, we have

$$I = Io\ [1 + m \cos (\Delta\varphi_R + \Delta\varphi)]$$

with $\Delta\varphi = \varphi\ (x + \delta x, y + \delta y) - \varphi\ (x,y)$, the phase difference due to the deformation of the object.
To solve these two equations and calculate $\Delta\varphi$ we can introduce a well-known optical phase ϕ_i in the set up by mounting a mirror of the Michelson interferometer on a piezo-electric translator.

By producing at least three phases ϕ_1, ϕ_2, ϕ_3, we can solve I_R and I and get $\Delta\varphi_R + \Delta\varphi$. By subtraction we calculate $\Delta\varphi$ and visualize the defect.
Figure 5 shows a defect of bonding in a composite material submitted to a thermal stressing.[7]
More sophisticated shearography systems can be used to study dynamic events (for example vibrating objects). In such cases, we have not enough time to use the phase stepping method to calculate $\Delta\varphi$. Also we calculate the Fourier transforms of the image of the object at two different times during the stressing (for example). To obtain enough good results, carrier fringes can also be produced between the two recording. But, finally pulsed TV-holography (or pulsed ESPI) gives better results than shearography !

a) use in fluid mechanics

Here again we use a laser source. The Wollaston prisms are replaced by a Michelson interferometer.
The advantage of using a Michelson interferometer mainly concerns the quantitative measurement. With the same principles as these described above for solid mechanic applications, we can get $\Delta\varphi$ (integrated through the phase object) for quasi-static or dynamic phase objects.

3. Conclusion

For solid mechanic applications (mainly non-destructive testing) some people said : shearography is very useful for on site industrial applications due to its relative insensitivity to air convection or turbulences and to ambiant vibrations. And they prove that by excellent experimental results. On another side, people working in the field of fluid mechanics said : shearography is very useful for its good sensitivity to air turbulences ! And they prove that by excellent experimental results too. That simply means that both communauties must discuss together (or must be informed each other on their work) to be less absolute in their arguments!

4 Outlook on the future

In many cases, digital shearing would give very exciting possibilities. Already, it is possible at a laboratory level to use TV-holography and a posteriori digital shearing in any direction with any amplitude to get appropriate shearograms.

References :

[1] Nomarski G. : French patent nr.1.059.103, May 1952
Nomarski G. : Differential microinterferometer with polarized light, J; de Phys. 16, 95-135, 1955

[2] Veret C. : quantitative schlieren for wind tunnel, ONERA report, N.T. 23, 1954

[3] Oertel H. : Differential interferometer for measurements in hypersonic shock tubes, ISL report T 17/61, 1961
Smeets G. : Differential interferometer for visualization and measurement of boundary layers, ISL report T 25/64, 1964

[4] George A. : Optical diagnostic of shock tube flows using differential interferometry. School of Aeronautics and Astronautics, West Lafayette, Perdue University, Indiana, USA, May 1997

[5] Desse J.M. : Recording and processing of interferograms by spectral characterization of the interferometric set-up, 6th National Congress on Visualization and Image Processing in Fluid Mechanics, Saint-Etienne, France, 1995

[6] Smigielski P. : Applications of coherent optics at ISL, seminar on Laser and Opto-electronic Technology in Industry, Xiamen, China, June 25-28, 1986, ISL report CO 228/86, 1986

[7] Smigielski P. : Industrial holography, Teknea ed., Toulouse, France, 1994

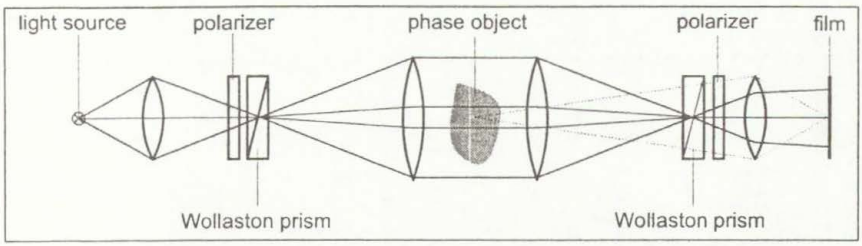

Fig.1. Differential interferometry in polarized light

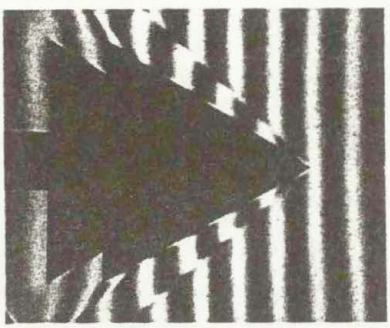

Fig.2. Rarefied supersonic flow in a shock tube. Light source : spark gap.

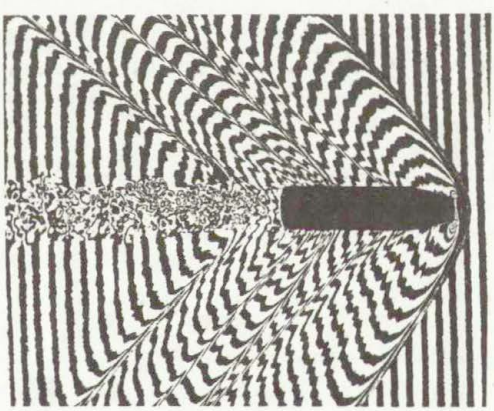

Fig. 3. Supersonic projectile in a ballistic range. Light source : pulse YAG laser

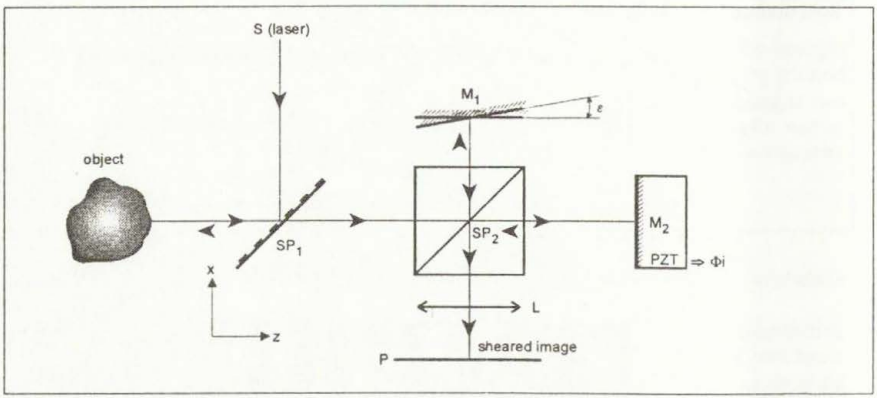

Fig. 4. Shearing with a Michelson interferometer

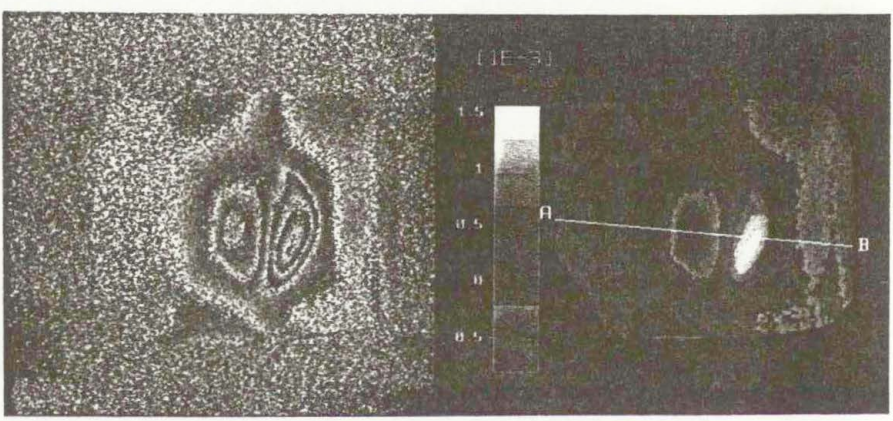

Fig. 5. Shearogram of a composite material showing a defect of bonding

2D IMAGES AND 3D OBJECT ANALYSIS AND RECOGNITION - AN INTELLIGENT APPROACH

Prof. Patrick Wang, Ph.D.
IAPR Fellow
College of Computer Science, Northeastern University
Boston, MA 02115, U.S.A.

pwang@ccs.neu.edu
http://www.ccs.neu.edu/home/pwang

Abstract

How do people learn and recognize things? These amazing capabilities have been taken for granted for years. Until recently, when one tries to use computers or machines to do things like recognizing handwritten characters, it becomes clear that such seemingly trivial tasks by human being turn out extremely difficult, if not impossible, by mechanical means such as computers.

After decades of rigorous attacks, such research is still as fresh as ever, and such mystery as for how human beings can do it remains largely unknown. In a sense, up to date, "human brain" is still the "smartest" or the "most intelligent" mechanism than any computer can provide.

In a way, the study of *pattern recognition* and *artificial intelligence* techniques has attracted more and more interests and attention. This talk intends to get some inside views of PR techniques using AI methodologies, and its applications to represent, learn, understand and recognize characters/words, one of the most popular, interesting, complicated and difficult languages in the world.

The speaker intends to conduct an on-line real time demo in this talk, on the internet: http://www.ccs.neu.edu/home/pwang/ObjectRecognition/